Combined optical and electrical modeling of polymer:fullerene bulk heterojunction solar cells

Jan D. Kotlarski,[1,a)] Paul W. M. Blom,[1] Lambert. J. A. Koster,[1,2] Martijn Lenes,[1,2] and Lenneke H. Slooff[3]
[1]*Molecular Electronics, Zernike Institute for Advanced Materials, University of Groningen, Nijenborgh 4, 9747 AG Groningen, Netherlands*
[2]*Dutch Polymer Institute, P.O. Box 902, 5600 AX Eindhoven, Netherlands*
[3]*Energy Research Centre of the Netherlands (ECN), P.O. Box 1, 1755 ZG Petten, Netherlands*

(Received 5 September 2007; accepted 11 February 2008; published online 16 April 2008)

Optical interference effects are important for the total absorption as well as the profile of the exciton generation rate in polymer:fullerene bulk heterojunction solar cells. For solar cells with an active layer of poly[2-methoxy-5-(3′,7′-dimethyloctyloxy)-1,4-phenylenevinylene] as electron donor and [6,6]-phenyl C_{61} butyric acid methyl ester as electron acceptor, the total exciton generation rate can be directly extracted from the saturated photocurrent. It is demonstrated that for solar cells with an active layer thickness smaller than 250 nm, a constant exciton generation profile, based on this extracted total rate, gives identical electrical characteristics as compared to exciton generation profiles from an optical model. For thicker cells interference effects have to be taken into account, since a uniform generation profile leads to an overestimation of recombination losses and space-charge formation. © *2008 American Institute of Physics*. [DOI: 10.1063/1.2905243]

I. INTRODUCTION

Plastic solar cells bear the potential for the realization of solar cells that are flexible, lightweight, inexpensive, and efficient. The efficient photoinduced electron transfer from a conjugated polymer to fullerene molecules[1] and the possibility to blend these materials in a so-called bulk heterojunction[2,3] (BHJ) have triggered a large scientific interest in solar cells based on these materials. In recent years several breakthroughs in efficiency have been reported. Mixing the conjugated polymer poly(2-methoxy-5-(3′,7′-dimethyloctyloxy)-p-phenylene vinylene) (MDMO-PPV) and methanofullerene [6,6]-phenyl C61-butyric acid methyl ester (PCBM) in a 1:4 weight ratio yielded a power conversion efficiency of 2.5%.[4] More recently, efficiencies in excess of 4% have been reported after optimizing the processing conditions of polymer:fullerene BHJ solar cells based on polythiophene derivatives as absorbing and electron donating material.[5–7] Using a low band gap polymer a power conversion efficiency of 5% has been currently achieved.[8] Also with regard to the understanding of the device operation of polymer:fullerene BHJ solar cells large progress has been made in recent years. Dissociation of electron-hole (e-h) pairs at the donor/acceptor interface is an important process that can limit the charge generation efficiency.[9] A balanced transport of electrons and holes in the blend is needed to suppress the buildup of space charge which, subsequently, will significantly reduce the power conversion efficiency.[10] Furthermore, the transport of electrons and holes in the blend needs to be enhanced in order to allow for fabrication of thicker films to maximize the absorption, without significant recombination losses.[11] Inclusion of the dissociation of bound electrons and holes at the donor/acceptor interface in a model based on the Poisson equation, current continuity equations and current equations (including both drift and diffusion), leads to a consistent description of the voltage and temperature dependence of the photocurrent of polymer:fullerene BHJ solar cells.[12] In this recently developed electrical model a constant profile has been assumed for the generation of excitons throughout the active layer.

Since a BHJ solar cell consists of a thin film layer stack of different materials on a transparent substrate, it has been recognized that optical interference effects might play an important role in the performance of solar cells and thus the assumption of a constant generation profile could be inaccurate. For this reason, an optical model has been developed initially for bilayer devices,[13] and subsequently also for BHJ solar cells.[14,15] These model calculations demonstrated that for MDMO-PPV:PCBM BHJ solar cells an oscillatory behavior in the total absorption as a function of active layer thickness is expected from optical interference effects. Furthermore, the exact shape of the exciton generation profile shows a strong dependence on active layer thickness. Similar conclusions were found for solar cells with a BHJ of poly(3-hexylthiophene) and PCBM in a 1:1 weight ratio.[16,17] However, a coupling between optical effects and solar cell parameters, such as short-circuit current J_{sc}, fill factor FF, and layer thickness L, is not straightforward. For MDMO-PPV:PCBM cells, for example, J_{sc} increases with increasing layer thickness due to an enhanced absorption, but the efficiency does not as a result of a decreasing FF due to space-charge formation and increased bimolecular recombination.[18] In order to incorporate optical effects in the solar cell performance, combined electrical and optical modeling has to be carried out. A first coupling between electrical and optical models has recently been made by Sievers *et al.*[19] They observed that interference effects, which affect the total exciton generation rate, do show up as an oscillatory behavior of J_{sc} as a

[a)]Electronic mail: barachem@yahoo.com.

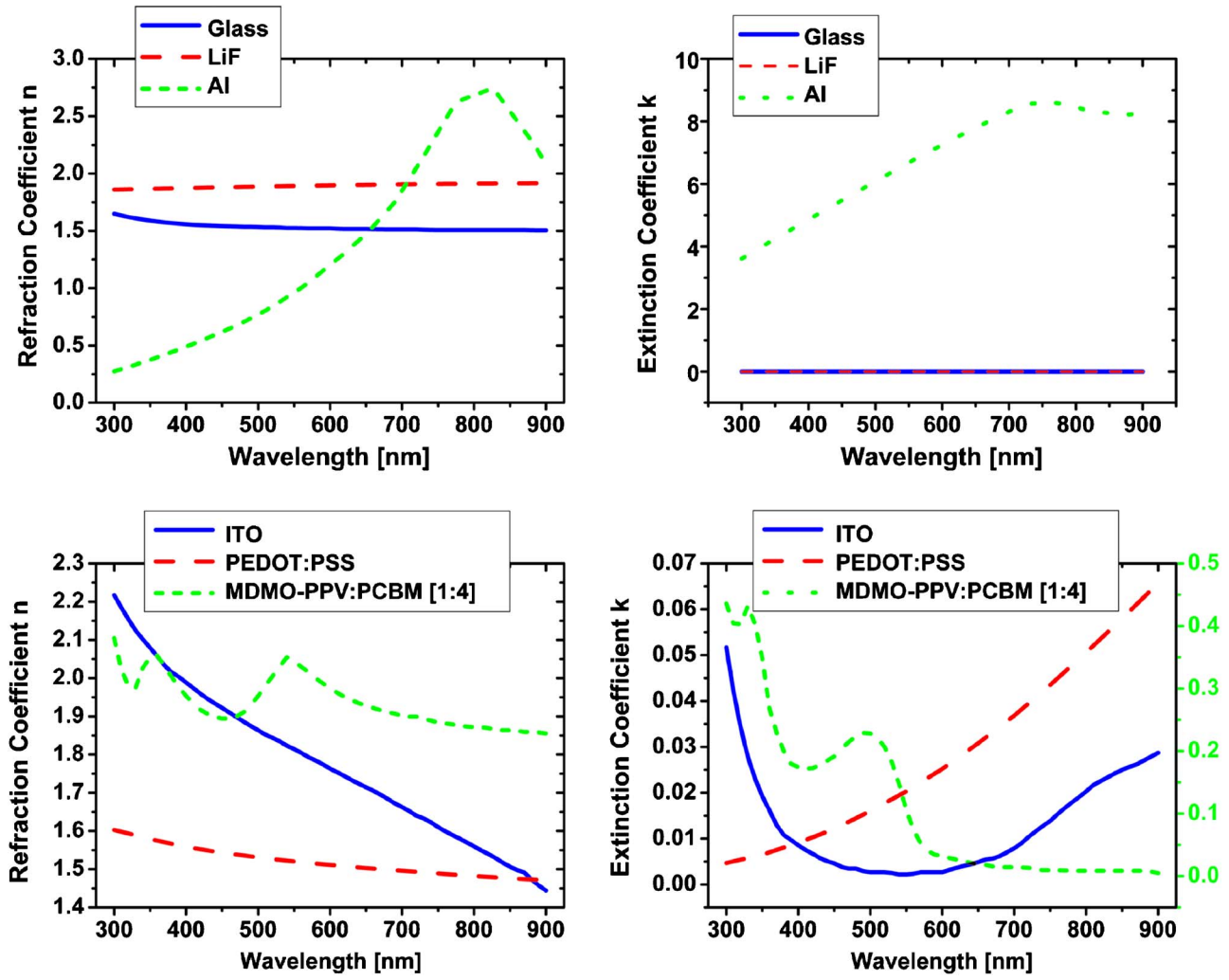

FIG. 1. (Color online) Optical parameters of glass, LiF, Al, ITO, PEDOT:PSS, and MDMO-PPV:PCBM as a function of wavelength.

function of active layer thickness. Similar findings were reported by Slooff *et al.* on BHJ solar cells based on a mixture of poly(9,9-didecanefluorene-alt-(bisthienylene) benzothiadiazole) and PCBM in a 1:4 weight ratio.[20] On the other hand, the exciton generation profile had no significant influence on solar cell performance.[19] This is in contrast with the conclusion that electrical models using a constant generation profile are not appropriate to model solar cell characteristics.[16] We demonstrate that solar cells with active layer thicknesses smaller than 250 nm can be correctly modeled solely from electrical data, without having to incorporate optical modeling. The variation of the total exciton generation rate with layer thickness is experimentally available from the saturated photocurrent at high reverse bias. The average constant exciton generation rate based on this total rate gives identical simulation results as obtained with incorporation of the optically modeled exciton generation profiles.

II. EXPERIMENTAL METHODS

As a first step the electrical characteristics of MDMO-PPV:PCBM solar cells are investigated as a function of active layer thickness. The solar cells are made by spin coating poly(3,4ethylenedioxythiophene)/poly(styrenesulphonic acid) (PEDOT:PSS) on top of a 0.6 mm thick glass substrate with patterned indium tin oxide (ITO) (140 nm) as a bottom contact. Subsequently, a blend of MDMO-PPV:PCBM (1:4 weight ratio) with varying thickness is spin coated on top of a nitrogen atmosphere. Finally, 0.5 nm of lithium fluoride (LiF) covered with 80 nm aluminium (Al) is evaporated as top contact. The current density-voltage (J-V) characteristics of these devices were measured in a nitrogen atmosphere under illumination by a white light halogen lamp calibrated with a silicon photodiode to simulate the AM 1.5 global solar spectrum, which is the spectrum assumed for the numerical simulations.

For the optical modeling of the glass substrate, the ITO electrode, and the MDMO-PPV:PCBM (1:4) blend, we used the optical constants as reported by Hoppe *et al.*[21] The values for PEDOT:PSS and LiF were determined with variable angle ellipsometry using a Woollam VASE ellipsometer. For Al standard literature values were used.[22] An overview of the optical constants for the various layers is shown in Fig. 1.

III. RESULTS

A. Saturated photocurrent

In Fig. 2 the measured dependence of the photocurrent density J_{ph} on the effective applied voltage $V=V_0-V_A$, which

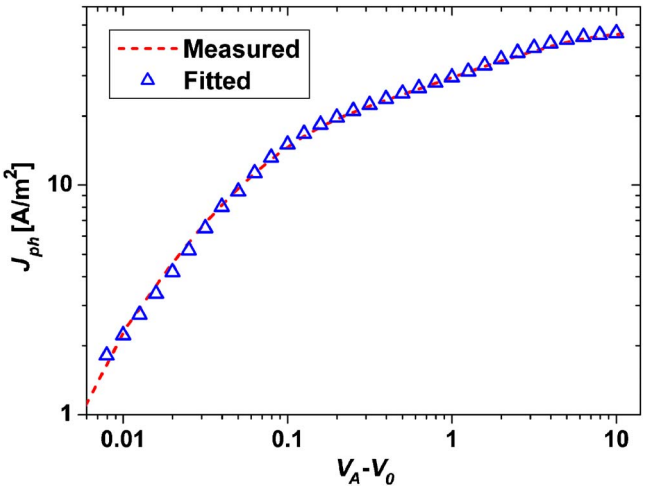

FIG. 2. (Color online) Measured (triangles) and simulated photocurrent (dashed line) as a function of effective applied voltage (V_A-V_0) for a solar cell with an active layer thickness of 128 nm. Note that the photocurrent at 10 V is near the saturated value.

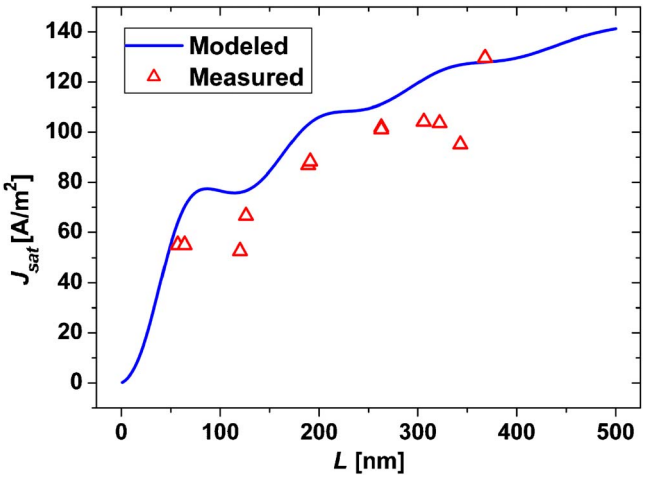

FIG. 3. (Color online) Experimental saturated photocurrent J_{sat} (triangles) and theoretical maximum photocurrent J_{max} (solid line) using the optically modeled total exciton generation rate and assuming a 100% internal quantum efficiency.

is a measure of the net electric field in the cell,[9] is shown for an active layer thickness of 128 nm. Here V_A is the applied voltage and V_0 is the compensation voltage defined as $J_{ph}(V_A=V_0)=0$. For V_A-V_0 up to 0.1 V we see a linearly increasing J_{ph}, resulting from the competition between drift and diffusion currents. For V_A-V_0 above 0.1 V, J_{ph}, tends to saturate as the slower increase of the drift-dominated current is limited by the maximum of the field-enhanced dissociation of the bound e-h pairs that are formed after the electron transfer from the donor to the acceptor.[9] At high reverse bias $V_A-V_0>10$ V all e-h pairs are dissociated and the photocurrent saturates to

$$J_{sat}=qG_{max}L, \tag{1}$$

where G_{max} is the maximum amount of bound e-h pairs that can be generated in the solar cell. It is evident that G_{max} is related to the total amount of absorbed light that governs the total exciton generation rate.

Also shown in Fig. 2 as a dashed line are the modeled $J_{ph}-V_A-V_0$ characteristics using our recently developed numerical device model.[12] In this model it is assumed that photogenerated excitons dissociate into bound e-h pairs, which only partially dissociate into free charges. The amount of free charges that is generated can be described by

$$G(T,E)=G_{max}P(T,E), \tag{2}$$

where $P(T,E)$ is the probability of separation of bound e-h pairs at the donor/acceptor interface. The photogeneration of free charge carriers can be described by the geminate recombination theory of Onsager.[23] Furthermore, it was pointed out by Braun that the dissociation probability is influenced by the fact that the bound electron-hole pair has a finite lifetime.[24] The probability that a bound polaron pair dissociates into free charge carries at a given electric field E and temperature T is then given by

$$P(T,E)=\frac{k_D(E)}{k_D(E)+k_F}, \tag{3}$$

with k_F denoting the rate constant as the bound electron-hole pair decays to its ground state, and $k_D(E)$ the rate constant for separation into free carriers, which is given by[24]

$$k_D=k_R\frac{3}{4\pi a^3}e^{-E_b/kT}\left[1+b+\frac{b^2}{3}+\frac{b^3}{18}+\frac{b^4}{180}+\cdots\right], \tag{4}$$

with a denoting the initial separation distance of the bound electron-hole pair at the interface, $b=e^3E/8\pi\varepsilon_0\varepsilon_r k^2T^2$, and E_b the binding energy of the electron-hole pair. Once separated, the charge carriers can again form a bound pair with a rate constant k_R. Using the Onsager theory for field dependent dissociation rate constants for weak electrolytes[25] for $k_D(E)$, Langevin recombination of free electrons and holes, and a Gaussian distribution of donor-acceptor distances, the generation rate of producing free electrons and holes depends on the charge carrier mobilities μ_n and μ_p of the electron and holes, respectively, the relative dielectric constant ε_r, the initial separation of e-h pairs a, and the ground state recombination rate k_F. As both the electric field distribution and the rate of charge separation are dependent on each other, an iterative algorithm is needed. We use a recently developed device program based on the electrical model described here.[12]

As a next step the total rate of exciton generation is calculated using an optical model following the transfer matrix approach developed by Knittl[26] and first utilized in organic photovoltaic devices by Petterson *et al.*[13] The calculated exciton generation rate is then transferred into a photocurrent J_{max} by assuming a 100% internal quantum efficiency in the solar cell. In Fig. 3 the experimentally determined J_{sat} is shown together with the calculated J_{max} as a function of solar cell active layer thickness L. As reported before, the calculated photocurrent following from the total exciton generation rate (J_{max}) increases in an oscillatory fashion with increasing active layer thickness, showing that the total exciton generation rate is influenced by the optical

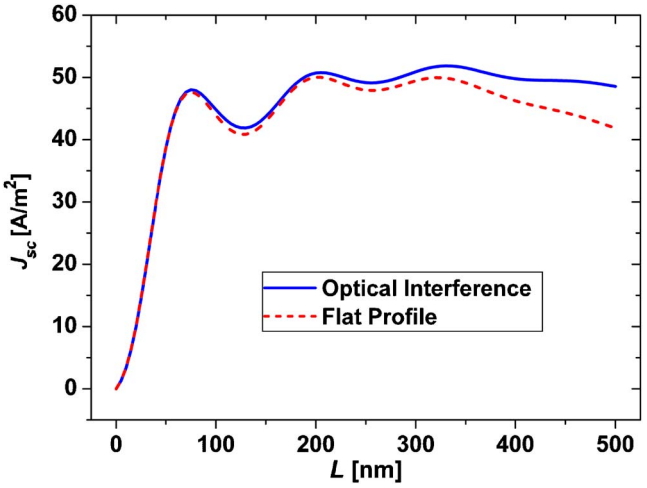

FIG. 4. (Color online) Simulated short-circuit currents using the calculated exciton generation rate profile $J_{sc}^{Profile}$ (solid line) or a constant average profile $J_{sc}^{Average}$ (dashed line) as a function of active layer thickness under 1000 W/m^2 AM 1.5 illumination.

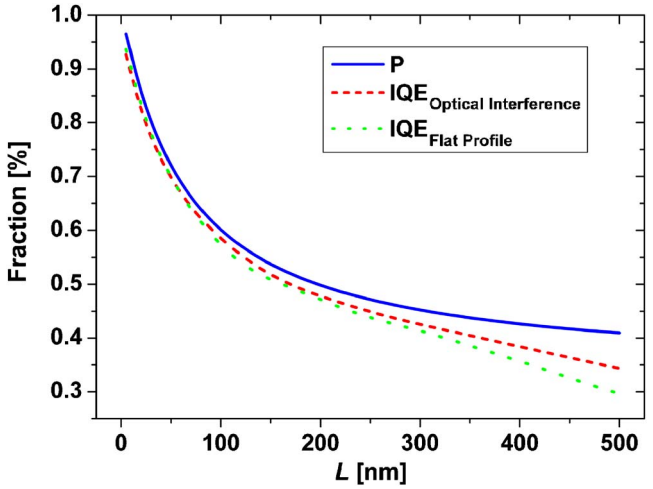

FIG. 5. (Color online) Average electron-hole pair dissociation probability $P(E,T)$ (solid line) and internal quantum efficiency at zero bias for the exciton generation rate profile $IQE_{sc}^{Profile}$ (dashed line) and the uniform profile $IQE_{sc}^{Average}$ (dotted line) as a function of active layer thickness.

interference in the layer stack. We also observe that the experimental J_{sat} follows the trend of J_{max}, but it is typically about 90% of its magnitude. This seems to indicate that of all created excitons about 90% are effectively transferred into charge carriers at high reverse bias. The missing 10% could be due to a combination of e-h pairs that are formed in "dead ends" of the phase separated morphology and limitations in charge transport. However, an alternative explanation could be that our materials have slightly different optical constants as compared to the reported values that we use in our calculations.[14] This could lead to a slight overestimation of the calculated absorption and is a subject of further study.

B. Influence of optical interference

Subsequently, the exciton generation profiles are calculated using the transfer-matrix approach: first calculating the intensity profile of each wavelength, then multiplying those results with the absorption of the active material, and then integrating those results over the relevant wavelength range (300 to 900 nm). These exciton generation profiles are then used as input for the electrical device model. The result is shown in Fig. 4 where the short-circuit current using the exciton generation rate profiles is shown ($J_{sc}^{Profile}$), together with the short-circuit current using an average exciton generation rate ($J_{sc}^{Average}$). The average exciton generation rate was chosen such that the total amount of generated excitons is identical to the amount of generated excitons for the profile. It is clear that for active layer thicknesses up to 250 nm the calculated $J_{sc}^{Profile}$ and $J_{sc}^{Average}$ are identical, as has also been reported by Sievers *et al.*, who calculated the J_{sc} up to layer thicknesses of 275 nm.[19] For layer thicknesses exceeding 300 nm we observe that $J_{sc}^{Profile}$ and $J_{sc}^{Average}$ clearly start to diverge. Thus, for solar cells with active layer thicknesses up to 275 nm the use of a constant exciton generation profile is justified for simulating the performance of MDMO-PPV:PCBM based solar cells. The variation of the total exciton generation rate with a layer thickness due to optical interference is taken into account by using the experimental J_{sat} as a measure for the total exciton generation rate.

Another interesting observation is that the calculated short-circuit currents follow the oscillatory behavior of the total absorption, but they do not further increase with increasing layer thickness. In Fig. 5 $J_{sc}^{Profile}/J_{max}$ and $J_{sc}^{Average}/J_{max}$, representing the internal quantum efficiency (IQE) under short-circuit condition, are plotted as a function of active layer thickness L. The internal quantum efficiency strongly decreases with increasing layer thickness. As stated above, the dissociation of bound e-h pairs is an important process in MDMO-PPV:PCBM BHJ solar cells.

In Fig. 5 the dissociation efficiency $P(E,T)$ is also shown at an electric field of V_{oc}/L as a function of L. By increasing the active layer thickness the electric field at short-circuit, typically given by V_{oc}/L with V_{oc} denoting the open-circuit voltage, is reduced, thereby reducing $P(E,T)$. Apart from that, as stated above, the dissociation efficiency also depends on the initial separation distance a (1.2 nm) of the bound electron and hole and the decay rate k_f (10^6 s^{-1}) of the bound e-h pair. Both have been determined from the voltage and temperature dependence of the photocurrent under reverse bias.[9] The agreement between $P(E,T)$ and IQE shows that the reduced e-h dissociation efficiency is the main origin for the reduction of J_{sc} for thick samples. The increasing difference between $P(E,T)$ and IQE for thick samples is a result of increasing recombination losses and a buildup of space charge.[18] For a 100 nm device the bimolecular recombination losses only amount to a few percent.[12]

C. Space charge and active layer thickness

In Fig. 4 it also appears that for thicknesses larger than 275 nm the $J_{sc}^{Profile}$ is lower than $J_{sc}^{Average}$, and that their difference increases with increasing thickness. In order to evaluate this difference we plot in Fig. 6 the exciton generation rate profile and its average as a function of distance x from the LiF/Al electrode for a 500 nm thick active layer. It appears that relatively more excitons are generated near the PEDOT-

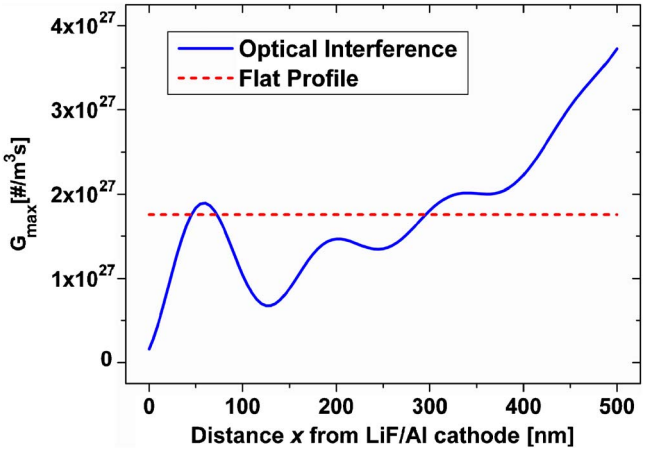

FIG. 6. (Color online) Simulated exciton generation rate profile (solid line) and its average (dashed line) as a function of distance x from the LiF/Al/cathode. Note the higher exciton generation rate near the anode (x =500 nm) for the exciton generation rate profile.

:PSS anode for the exciton generation profile as compared with its average. So in the case of the generation profile, the holes, which have a lower mobility than the electrons, are created close to the contact where they are extracted. This will reduce the amount of holes that are lost during transport due to bimolecular recombination and thus will enhance the efficiency. Furthermore, the buildup of space charge will be less in case the exciton generation profile is taken as initial distribution.

To demonstrate this reduction of space charge, we simulated the photocurrent for both the exciton generation rate profile and its average as a function of $V_A - V_0$ for a 500 nm thick active layer, as shown in Fig. 7. This shows that the buildup of space charge is less severe for the exciton generation rate profile than for its average.

IV. CONCLUSIONS

In conclusion, we have shown that the average exciton generation rate of MDMO:PCBM devices can be experimentally extracted from the saturated photocurrent at high reverse bias. For MDMO:PCBM devices under these conditions the total amount of generated excitons is close to the total amount of extracted charges. The variation of the total exciton generation rate with active layer thickness due to interference is then automatically taken into account. The device operation parameters (J_{ph}, J_{sc}, and IQE) for solar cells with active layers thinner than 250 nm show no significant difference when either an exciton profile as obtained from optical modeling is used or a constant exciton generation rate profile, provided that the total exciton generation rate of both profiles are the same. For devices with active layers thicker than 300 nm it is important to include the optical exciton generation profiles. The losses due to bimolecular recombination and space-charge formation become both dependent on the initial position of the slowest carrier, which are holes in the case of MDMO:PCBM devices.

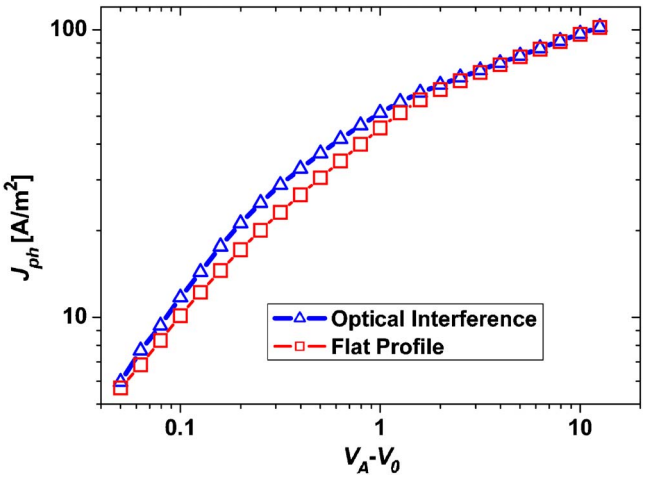

FIG. 7. (Color online) Photocurrent J_{ph} as a function of effective voltage $V_A - V_0$ for the exciton generation rate profile (triangles with solid line) and its average (squares with dashed line) for an active layer thickness of 500 nm.

[1]N. S. Sariciftci, L. Smilowitz, A. J. Heeger, and F. Wudl, Science **258**, 1474 (1992).
[2]J. J. M. Halls, C. A. Walsh, N. C. Greenham, E. A. Marseglia, R. H. Friend, S. C. Moratti, and A. B. Holmes, Nature (London) **376**, 498 (1995).
[3]G. Yu, J. Gao, J. C. Hummelen, F. Wudl, and A. J. Heeger, Science **270**, 1789 (1995).
[4]S. E. Shaheen, C. J. Brabec, N. S. Sariciftci, F. Padinger, T. Fromherz, and J. C. Hummelen, Appl. Phys. Lett. **78**, 841 (2001).
[5]F. Padinger, R. S. Rittberger, and N. S. Sariciftci, Adv. Funct. Mater. **13**, 85 (2003).
[6]G. Li, V. Shrotriya, J. Huang, Y. Yao, T. Moriarty, K. Emery, and Y. Yang, Nat. Mater. **4**, 864 (2005).
[7]W. Ma, C. Yang, X. Gong, K. Lee, and A. J. Heeger, Adv. Funct. Mater. **15**, 1617 (2005).
[8]J. Peet, J. Y. Kim, N. E. Coates, W. L. Ma, D. Moses, A. J. Heeger, and G. C. Bazan, Nat. Mater. **9**, 497 (2007).
[9]V. D. Mihailetchi, L. J. A. Koster, J. C. Hummelen, and P. W. M. Blom, Phys. Rev. Lett. **93**, 216601 (2004).
[10]V. D. Mihailetchi, L. J. A. Koster, J. C. Hummelen, and P. W. M. Blom, Phys. Rev. Lett. **94**, 126602 (2005).
[11]M. M. Mandoc, L. J. A. Koster, and P. W. M. Blom, Appl. Phys. Lett. **90**, 133504 (2007).
[12]L. J. A. Koster, E. C. P. Smits, V. D. Mihailetchi, and P. W. M. Blom, Phys. Rev. B **72**, 085205 (2005).
[13]A. A. Petterson, L. S. Roman, and O. Inganäs, J. Appl. Phys. **86**, 487 (1999).
[14]H. Hoppe, N. Arnold, N. S. Sariciftci, and D. Meissner, Sol. Energy Mater. Sol. Cells **80**, 105 (2003).
[15]N.-K. Persson, H. Arwin, and O. Inganas, J. Appl. Phys. **97**, 034503 (2005).
[16]A. J. Moulé, J. B. Bonekamp, and K. Meerholz, J. Appl. Phys. **100**, 094503 (2006).
[17]H. Hoppe, S. Shokhovets, and G. Gobsch, Phys. Status Solidi (RRL) **1**, 40 (2007).
[18]M. Lenes, L. J. A. Koster, V. D. Mihailetchi, and P. W. M. Blom, Appl. Phys. Lett. **88**, 243502 (2006).
[19]D. W. Sievers, V. Shrotriya, and Y. Yang, J. Appl. Phys. **100**, 114509 (2006).
[20]L. H. Slooff, S. C. Veenstra, J. M. Kroon, D. J. D. Moet, J. Sweelssen, and M. M. Koetse, Appl. Phys. Lett. **90**, 143506 (2007).
[21]H. Hoppe, N. S. Sariciftci, and D. Meissner, Mol. Cryst. Liq. Cryst. Sci. Technol., Sect. A **385**, 113 (2002).
[22]D. R. Lide, *Handbook of Chemistry and Physics* (CRC, Boca Raton, 1994).
[23]L. Onsager, Phys. Rev. **54**, 554 (1938).
[24]C. L. Braun, J. Chem. Phys. **80**, 4157 (1984).
[25]L. Onsager, J. Phys. Chem. **2**, 599 (1934).
[26]Z. Knittl, *Optics of Thin Films* (Wiley, London, 1976).